

Distributed Transmit Beamforming: Design and Demonstration from the Lab to UAVs

Samer Hanna, *Student Member, IEEE*, and Danijela Cabric, *Fellow, IEEE*

Abstract—Cooperating radios can extend their communication range by adjusting their signals to ensure coherent combining at a destination radio. This technique is called distributed transmit beamforming. Beamforming (BF) relies on the BF radios having frequency synchronized carriers and phases adjusted for coherent combining. Both requirements are typically met by exchanging preambles with the destination. However, since BF aims to increase the communication range, the individually transmitted preambles are typically at low SNR and their lengths are constrained by the channel coherence time. These noisy preambles lead to errors in frequency and phase estimation, which result in randomly changing BF gains. To build reliable distributed BF systems, the impact of estimation errors on the BF gains need to be considered in the design. In this work, assuming a destination-led BF protocol and Kalman filter for frequency tracking, we optimize the number of BF radios and the preamble lengths to achieve reliable BF gain. To do that, we characterize the relations between the BF gains distribution, the channel coherence time, and design parameters like the SNR, preamble lengths, and the number of radios. The proposed relations are verified using simulations and via experiments using software-defined radios in a lab and on UAVs.

Index Terms—Distributed transmit beamforming, cooperative communications, UAVs

I. INTRODUCTION

Distributed transmit beamforming (BF) enables a group of radios to act as a virtual antenna array when transmitting a common message to a destination radio. By having N equal power radios beamform, the received power at the destination can increase by up to N^2 ; N -fold due to transmit power increase and N -fold due to coherent combining [1]. The N^2 increase can theoretically provide up to N fold extension of communication range [2]. Thus, BF can enable long-range communications from cooperating low power devices, unable to communicate individually with a remote destination. This can be useful for power-constrained sensor networks [3] or UAVs deployed in remote regions [4].

For separate radios to act as one virtual array, they need to synchronize their carrier frequencies and adjust their phases for coherent combining at the destination. Both requirements are typically satisfied by exchanging preambles with the destination for channel phase estimation and carrier frequency synchronization [2]. However, given that in typical BF scenarios the radios have low power and/or the destination is

remote, the pre-BF SNR of individual radios is low, and there are errors in both channel estimation and destination-led frequency synchronization, which result in phase errors in the combining signals. These combining phase errors will lead to the BF gains being non-deterministic and less than N^2 . The BF gain degradation cannot always be mitigated, especially in high mobility radios like UAV-mounted, where the channel coherence time limits the preamble lengths and makes the combining phase errors inevitable. To build a reliable BF system despite of these errors, we need to specify the number of BF radios and the preamble lengths such that a minimum desired post-BF SNR is attained with a given probability.

Existing works have proposed many approaches for BF leveraging different methods for phase adjustment and frequency synchronization [3]. Approaches for phase adjustment include explicit channel feedback from the destination [5], 1-bit feedback where the BF radios iteratively adjust their phase based on binary feedback from the destination [6], and roundtrip message exchange among the destination and BF radios [7]. Other works proposed using the BF radios' placements to adjust the phase [8], however, this only works in a line-of-sight channel. For frequency synchronization, some works have relied on external frequency references like GPS [9], [10], out of band signaling [11], and others relied on a destination preamble along with using the extended Kalman filter (EKF) for tracking the carrier drift [12]. While these works have proposed interesting approaches, the relation between the BF gains and the pre-BF SNR, necessary for designing a reliable BF system, was not analyzed.

Using the aforementioned approaches, several BF demonstrations were carried; in a controlled lab experiment, 1-bit feedback was demonstrated using EKF for frequency synchronization in [12], [13] and out-of-band signaling in [11]. Outdoor ground based demonstrations spanning several kilometers using explicit channel feedback were performed in [9], [10] relying on GPS for frequency synchronization. Using explicit feedback, in [4], BF was demonstrated from UAVs with the synchronization performed over wires attached to the flying UAVs. These works have shown the potentials for BF in signal combining, yet their results are hard to generalize to different scenarios because they are mostly empirical.

In this paper, we consider a destination-led BF protocol using the Kalman filter (KF) for synchronization and explicit channel feedback. For that protocol, assuming equal pre-BF SNRs, we propose an analytical framework relating the statistical distribution of the BF gains, with the system parameters including pre-BF SNR, the number of BF radios, and the duration of the exchanged preambles. Using this framework,

The authors are with the Electrical and Computer Engineering Department, University of California, Los Angeles, CA 90095, USA. e-mail: samerhanna@ucla.edu, enesk@g.ucla.edu, danijela@ee.ucla.edu.

This work was supported in part by NSF under grant 1929874 and by the CONIX Research Center, one of six centers in JUMP, a Semiconductor Research Corporation (SRC) program sponsored by DARPA.

for a given channel coherence time, we optimize the number of radios and the length of the preambles for the BF gain to exceed a minimum SNR with a given probability, thus creating a reliable BF system. To derive this framework, we derive the variance of the combining phase errors, which depends on the preamble lengths and the pre-BF SNR. Then, given the variance of the combining phase errors, we approximate the distribution of the BF gains. The proposed framework is verified using simulations and experimentally using two BF software-defined radios (SDRs) in a lab environment. To the best of our knowledge, we are the first to demonstrate fully wireless BF from flying UAVs without any wires attached. Our main contributions are:

- We proposed an analytical framework describing the relations between the BF gains and the pre-BF SNR, the length of the preambles, and the number of BF radios for a destination-led BF protocol under the assumption of equal pre-BF SNRs. These relations were verified using simulations and experimentally using two BF software-defined radios.
- We characterized the distribution of BF gains assuming zero-mean normally distributed phase errors. We derived the variance of the BF gains. For large N , we proved the BF gain distribution approaches Gaussian and for small phase error variance we approximated it using a Gamma distribution.
- Using the BF framework, we proposed an approach to determine the minimum number of BF radios and the shortest BF preambles to meet a minimum post-BF SNR with a given probability and verified that it meets the requirements using simulations.

II. SYSTEM MODEL AND DISTRIBUTED BF PROTOCOL

A. System Model

Consider N identical radios collaborating to beamform a message to a destination radio D in a narrowband flat-fading channel. The BF radios can be remotely deployed Internet-of-Things devices communicating with a gateway or UAVs communicating with a ground station. The message is encoded in the complex baseband signal $m(t)$, which is assumed to have unity power. The n -th radio transmits a signal $z_n(t)$ and the combined baseband signal at the destination is given by

$$y(t) = \sum_{n=1}^N a_n z_n(t) \exp\{j(2\pi f_n t + \phi_n)\} + w(t) \quad (1)$$

where between the destination and the n -th radio, a_n is the channel amplitude, f_n is the carrier frequency offset, and ϕ_n is the phase offset. The white Gaussian noise process is given by $w(t)$ and has power spectral density $N_0/2$. The phase and frequency offsets result from the lack of synchronization between the local oscillators of the radios, the wireless propagation environment, and the Doppler frequency offsets resulting from the relative motion of radios. While these phenomena make the phase and frequency offsets time varying, we assume that the message is shorter than the resulting channel coherence time and we approximate them as constant for one message.

For the signal $m(t)$ to combine coherently at the destination, the BF radios need to compensate for the phase and frequency offsets before transmission. The compensated signal transmitted by radio n , thus, is given by

$$z_n(t) = m(t) \exp\{-j(2\pi \hat{f}_n t + \hat{\phi}_n)\} \quad (2)$$

where \hat{f}_n and $\hat{\phi}_n$ are the n -th radio estimates of the frequency and phase offsets obtained through the BF protocol, which is described later. The received signal can be rewritten as

$$y(t) = m(t) \sum_{n=1}^N a_n \exp\{j\phi_n^e(t)\} + w(t) \quad (3)$$

where the combining phase error from radio n at instant t is given by

$$\phi_n^e(t) = (2\pi(f_n - \hat{f}_n)t + (\phi_n - \hat{\phi}_n)) \quad (4)$$

Due to residual frequency errors, the combining phase error increases with time. However, we are only interested in evaluating the BF gain during the payload. Considering the evaluation instance to be t_e seconds after the phase estimation, we get $\phi_n^e = \phi_n^e(t_e)$. The beamforming gain at instant t_e can be defined as the ratio between the energy of the combined signals to that of the individual transmissions

$$G = \frac{\|\sum_{n=1}^N a_n \exp\{j\phi_n^e\}\|^2}{\sum_{n=1}^N a_n^2} \quad (5)$$

Each BF radio is assumed to transmit at its maximum power level P_T , which is common to all radios. We also assume that the BF radios are deployed in proximity from each other far from the destination, and hence they experience similar signal attenuation. Given these assumptions, we get $a_n = a$ for all n , where a is the path loss. In that case, G simplifies to [14]

$$G = \frac{1}{N} \left| \sum_{n=1}^N \exp\{j\phi_n^e\} \right|^2 \quad (6)$$

The pre-BF SNR at the destination from one radio is given by

$$\gamma_{\text{preBF}} = \frac{a^2 P_T}{N_0} \quad (7)$$

and the post-BF SNR of the combined signal from all N BF radios is equal to

$$\gamma_{\text{postBF}} = N \gamma_{\text{preBF}} G \quad (8)$$

The signals transmitted by the destination to the BF radios experience an SNR given by

$$\gamma_{\text{DR}} = \frac{a^2 P_T^D}{N_0} \quad (9)$$

where the destination has a transmit power P_T^D . The destination transmit power is assumed to be equal to or larger than that of the BF radios, that is $P_T^D \geq P_T$. Note that the post-BF SNR follows the same distribution of G , which we need to know to realize a minimum post-BF SNR with a given probability. As for G , it depends on ϕ_n^e , which results from the estimation errors during the BF protocol.

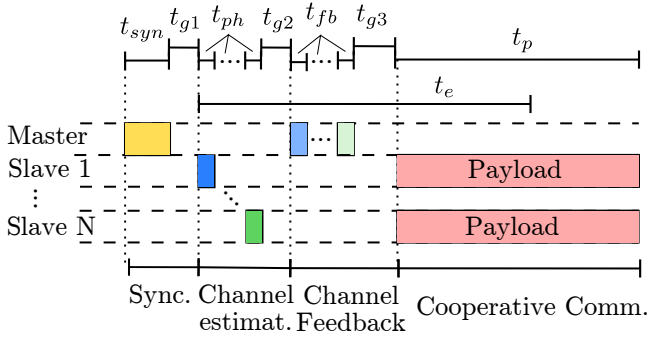


Fig. 1: Timing diagram of BF protocol. The destination is the master and BF radios are the slaves.

B. Beamforming Protocol

We start by describing the BF protocol, which aims to provide each BF radio with estimates of its phase and frequency offsets $\hat{\phi}_n$ and \hat{f}_n . We consider a master-slave beamforming protocol; the destination radio is used as a master since it has a larger transmit power and the slaves are the beamforming radios. The master initiates the beamforming procedure and sends a preamble for frequency synchronization. After correcting their frequencies, the slaves send a channel estimation preamble to the master. The master calculates a phase estimate $\hat{\phi}'_n$ and transmits it back to the slaves that receive a slightly different value $\hat{\phi}_n$ due to feedback errors. Once each slave knows $\hat{\phi}_n$ and \hat{f}_n , they can start transmitting their payload.

In Fig. 1, we illustrate the transmitted signals. All the signaling is performed on the same frequency band, hence, all transmissions are received by all radios. The different beamforming stages can be described as follows

- 1) Synchronization: The master sends a synchronization preamble of duration t_{syn} . Using this signal each slave estimates its frequency offset \hat{f}_n . This preamble is also used as a time reference. A guard time of duration t_{g1} is provided for the slaves to process the signals.
- 2) Channel Estimation: Each slave during an allocated time slot sends a channel estimation preamble of duration t_{ph} . The master estimates $\hat{\phi}'_n$ from each slave. A guard time t_{g2} is used.
- 3) Channel Feedback: The master sends $\hat{\phi}'_n$ back to the slaves and due to feedback error each slave receives a slightly different phase estimate $\hat{\phi}_n$. A guard time t_{g3} is used.
- 4) Cooperative Communication: After estimating \hat{f}_n and receiving $\hat{\phi}_n$, all slaves adjust their signals accordingly and transmit their payload of duration t_p .

The duration of the BF overheads incurred by the protocol is given by

$$t_{\text{ov}} = t_{\text{syn}} + N(t_{\text{ph}} + t_{\text{fb}}) + t_{g1} + t_{g2} + t_{g3} \quad (10)$$

All the signal processing is assumed to be done in discrete time domain, hence all the time durations are assumed to be an integer multiple of the sampling time T_s . The time overhead can be written in terms of samples as

$$N_{\text{ov}} = N_{\text{syn}} + N(N_{\text{ph}} + N_{\text{fb}}) + N_{g1} + N_{g2} + N_{g3} \quad (11)$$

where N_{ov} is defined as $N_{\text{ov}} = t_{\text{ov}}/T_s$ and the remaining number of samples are defined similarly. As we can see from (11), the beamforming overheads scale with the number of BF radios N . For short coherence time channels, the overheads N_{ov} are typically constrained, and to increase N while keeping N_{ov} constant, the duration of the preambles needs to be reduced. Note that we assume that the payload is already shared among all the slaves. This can be achieved using a network broadcasting protocol [15], which we do not discuss in this work. As for the guard time, it is dependent on the implementation of the BF protocol. A more optimized implementation using an FPGA for instance would require shorter guard times than an implementation using a general purpose processor. Also, note that cooperative communication only requires the BF radios to be synchronized with each other and not necessarily with the destination. However, in order to use channel estimates from the destination, they need to be synchronized with the destination.

Since BF is used to improve the SNR where the individual pre-BF SNR is low, the estimation errors within the protocol can not be neglected and will lead to a combining phase error ϕ_n^e as given by (4). At the evaluation time t_e , the variance of the combining phase error σ_e^2 defined as $\text{var}\{\phi_n^e\}$ is given by

$$\sigma_e^2 = (2\pi t_e)^2 \sigma_f^2 + \sigma_{ph}^2 + \sigma_{fb}^2 \quad (12)$$

where the frequency estimation variance is given by $\sigma_f^2 = \text{var}\{f_n - \hat{f}_n\}$, the phase estimation and feedback variances are given by $\sigma_{ph}^2 = \text{var}\{\phi_n - \hat{\phi}'_n\}$ and $\sigma_{fb}^2 = \text{var}\{\hat{\phi}'_n - \hat{\phi}_n\}$ respectively.

In the following Sections, III and IV, we discuss the waveforms and estimators used for frequency estimation and phase estimation & feedback respectively. We provide expressions for their error variances in terms of the pre-BF SNR and the preamble lengths. We argue that the resulting phase errors follow a zero-mean Gaussian distribution. For zero-mean Gaussian distributed phase errors with variance σ_e^2 , we approximate the distribution of the BF gain in Section V to complete the BF framework. This framework is numerically and experimentally verified in Section VI. After verifying the framework, we show how it can be used for designing BF systems in Section VII. The BF design procedures are illustrated using example scenarios in Section VIII.

III. FREQUENCY SYNCHRONIZATION

The objective of frequency synchronization is to eliminate the frequency offset between the destination and the BF radios. We start by discussing the signals used for synchronization and the proposed oneshot estimator and its variance. Then we discuss frequency tracking using Kalman filter assuming multiple successive BF cycles.

A. Frequency Offset Estimation

For frequency synchronization, we use a preamble consisting of N_{ZC} repetition of a Zadoff-Chu (ZC) sequence of length

TABLE I: Kalman Filter relations

Model	
$x_k = x_{k-1} + w_{k-1}$	(15)
$z_k = x_k + v_k$	(16)
Update	
$K_k = \frac{p_{k k-1}}{p_{k k-1} + r}$	(17)
$x_{k k} = x_{k k-1} + K_k(z_k - x_{k k-1})$	(18)
$p_{k k} = (1 - K_k)p_{k k-1}$	(19)
Predict	
$x_{k+1 k} = x_{k k}$	(20)
$p_{k+1 k} = p_{k k} + q$	(21)

M similar to [16], satisfying $N_{\text{syn}} = N_{\text{ZC}}M$. The frequency estimator calculates the auto-correlation statistic

$$\eta_f = \sum_{k=0}^{(N_{\text{ZC}}-)M-1} y_f^*[k]y_f[k+M] \quad (13)$$

where $y_f[k]$ is the noisy received preamble with the frequency offset, and $()^*$ denotes the conjugate operator. The frequency offset estimate at slave n is thus given by $\hat{f}_n = \frac{1}{2\pi T_s M} \angle \eta_f$ where $\angle(\cdot)$ denotes the phase of a complex number calculated using arctan. The term $\angle \eta_f$ calculates the phase difference between two successive sequence repetitions, under the assumption that M is small such that no phase wrapping occurs. The error variance for this estimator is given by [17, eq.70]

$$\sigma_{f_e}^2 = \left(\frac{1}{M(N_{\text{ZC}}-1)^2 \gamma_{\text{DR}}} + \frac{1}{2M(N_{\text{ZC}}-1) \gamma_{\text{DR}}^2} \right) \frac{1}{(2\pi M T_s)^2} \quad (14)$$

This estimator is unbiased thus $\mathbb{E}\{\hat{f}_n - f_n\} = 0$ and was derived using a linear approximation of the arctan assuming η_f has a high SNR. By choosing M to be large, using the central limit theorem, the distribution of η_f can be approximated by Gaussian, thus making $\hat{f}_n - f_n$, which is approximated as linear in η_f , a zero mean Gaussian RV. However, at low SNR of η_f , $\angle \eta_f$ becomes uniform and the expression of $\sigma_{f_e}^2$ no longer applies. This regime can be avoided by increasing N_{ZC} , otherwise, the BF gains will be too low to be of practical importance. Note that in practice the frequency offset is correlated among successive packets with short separation. This estimator, referred to as a oneshot frequency estimator, does not benefit from this correlation.

B. Interpacket Frequency Tracking using Kalman Filter

If beamforming is performed periodically at a fixed cycle duration t_{cyc} shorter than the channel coherence time, the frequency estimates between packets at each slave are correlated. Kalman filter (KF), thus, can be used to track the frequency to reduce the estimation variance. The drift system model and the KF equations are given in Table I for one BF radio following the conventional KF notation [18]. The frequency process drift and measurement models are given by (15) and

(16), respectively, where x_k is the true frequency value in Hz (previously denoted by f_n) and z_k is the measured frequency at time kt_{cyc} . The noise terms for the process w_k and the measurement v_k are assumed to be zero mean Gaussian RV and their variances are q and r respectively. For the KF update equations, at step k , K_k is the Kalman gain, $x_{k|k-1}$ is the prediction of x and $p_{k|k-1}$ is the error variance given z_{k-1} . The value of $x_{k|k}$ is the predicted frequency offset and $p_{k|k}$ is its error variance given z_k .

By substituting (17) in (18) and using (20) we get

$$x_{k|k} = \frac{r}{p_{k|k-1} + r} x_{k-1|k-1} + \frac{p_{k|k-1}}{p_{k|k-1} + r} z_k \quad (22)$$

from which we can see that the KF creates a weighted average between the previous prediction and the current measurement. The weights of this average are based on the predicted process variance $p_{k|k-1}$ and the measurement variance r . The larger the process variance relative to the measurement variance, the more weight is given to the measured value and vice versa. Since (22) is a linear equation, if z_k is a zero mean Gaussian RV, the output of KF will also be zero-mean and Gaussian. For BF, we are interested in calculating the KF error variance.

Proposition 1: The steady state frequency estimation error variance of KF from Table I is

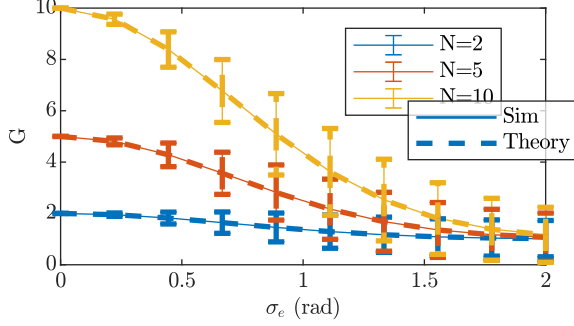
$$\sigma_{f_k}^2 = \frac{-q + q\sqrt{1 + 4\frac{r}{q}}}{2} \quad (23)$$

The proof is in Appendix A. Using (23) and assuming the system variances are accurately known, we argue that KF never increases the error variance. By rewriting (23), as $\sigma_{f_k}^2 = \frac{-q + \sqrt{q^2 + 4qr}}{2}$, we can see that $\sigma_{f_k}^2$ is non-decreasing in q and if $q = 0$, at convergence the error variance $\sigma_{f_k}^2 = 0$ for any r . For $q \gg r$, r/q is small and using the approximation $\sqrt{1 + 4\frac{r}{q}} \approx 1 + 2\frac{r}{q}$, we get $\sigma_{f_k}^2 = r$. Thus if q and r are perfectly known, the error variance reduction due to KF is higher for large r/q and, in the worst case scenario for small r/q , KF will give the measurement variance $\sigma_{f_k}^2 = r$, as if we did not use KF. However, if the values of q and r used in KF do not match the system, this result does not hold and KF might deteriorate the frequency estimation. Note that the extended KF (EKF) can track both phase and frequency and might yield a smaller variance than KF which only tracks the frequency. However, EKF can diverge due to phase wrapping [13], which is not desirable in a reliable BF system, and thus was not considered in this work.

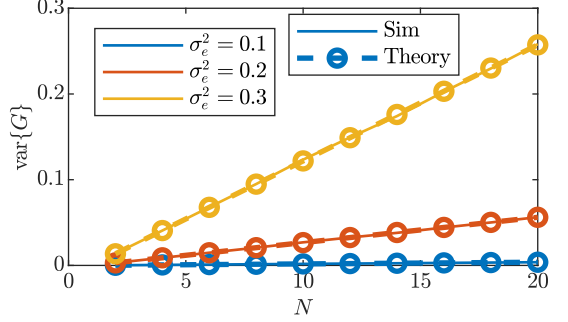
IV. PHASE ESTIMATION AND FEEDBACK

The objective of the phase estimation and feedback is to have the slaves modify their signals to ensure coherent combining at the destination. In the phase estimation stage, each slave transmits a known signal $x_{\text{ph}}[n]$ consisting of N_{ph} samples. The master receives the noisy signal $y_{\text{ph}}[k]$. The proposed estimator calculates the correlation $\eta_{\text{ph}} = \sum_{k=0}^{N_{\text{ph}}-1} x_{\text{ph}}[k]y_{\text{ph}}[k]$, from which the phase estimate is calculated using $\hat{\phi}'_n = \angle \eta_{\text{ph}}$. The variance of this estimator is given by [19]

$$\sigma_{p_{he}}^2 = \frac{1}{2N_{\text{ph}}\gamma_{\text{preBF}}} \quad (24)$$



(a) The mean BF Gain and its standard deviation as error bars.

(b) The relation between the BF variance and N for fixed σ_e^2 .Fig. 2: The relation between BF gain, N , and σ_e^2 .

where $N_{\text{ph}}\gamma_{\text{preBF}}$ is the SNR of η_{ph} . The phase error $\hat{\phi}'_n$ follows a zero mean Gaussian distribution as long as the SNR of $\eta_{\text{ph}} \gg 1$ [19], which is the regime of interest.

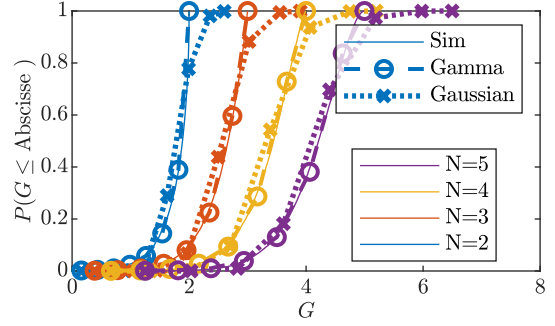
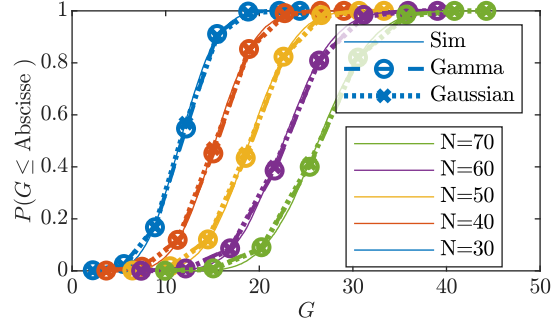
As for the phase feedback, we use in-band feedback where the value of $\hat{\phi}'_n$ is encoded in the phase difference between two identical preambles to counter hardware phase ambiguity. Let the phase feedback preamble be given as a vector $\mathbf{x}_{\text{fbp}} \in \mathbb{C}^{N_{\text{fb}}}$. The master transmits the sequence

$$\mathbf{x}_{\text{fb}} = [\mathbf{x}_{\text{fbp}}^T \quad \mathbf{x}_{\text{fbp}}^T e^{j\hat{\phi}'_1} \dots \mathbf{x}_{\text{fbp}}^T e^{j\hat{\phi}'_n} \dots \mathbf{x}_{\text{fbp}}^T e^{j\hat{\phi}'_N}]^T \quad (25)$$

Once received as $y_{\text{fb}}[k]$ with added noise, slave n estimates the phase difference between the first preamble and the n -th preamble using the statistic $\eta_{\text{fb}} = \sum_{k=0}^{N_{\text{fb}}-1} y_{\text{fb}}[k]y_{\text{fb}}^*[k+nN_{\text{fb}}]$ and calculates the angle $\hat{\phi}'_n = \angle \eta_{\text{fb}}$. The variance of the feedback is similar to that used for frequency estimation in (14) (with $N_{\text{ZC}} = 2$, $M = N_{\text{fb}}$) and is given by

$$\sigma_{f_{be}}^2 = \left(\frac{1}{N_{\text{fb}}\gamma_{\text{DR}}} + \frac{1}{2N_{\text{fb}}\gamma_{\text{DR}}^2} \right) \quad (26)$$

Note that there are other ways to feedback the phase estimates, however, this approach is simple to implement. Another alternative was to encode the values of $\hat{\phi}'_n$ as floating-point numbers and transmit them using digital modulation. However, since we are considering a low SNR and a mistake in one of the most significant bits can be detrimental, we would need to implement channel coding. This would add unnecessary complexity to our protocol.

(a) The distribution of G for small N and small $\sigma_e^2 = 0.1$.(b) The distribution of G for large N and large $\sigma_e^2 = 1$.Fig. 3: The distribution of G for different N and σ_e^2

V. BEAMFORMING GAIN ANALYSIS

In this section, our objective is to approximate the distribution of G , assuming that the ϕ'_n are independent Gaussian random variables (RVs) with zero mean and variance σ_e^2 . The Gaussian assumption applies to our protocol because the errors of the proposed estimators are independent and can be approximated by a zero-mean Gaussian RVs. Hence, their sum according to (4) is also zero-mean Gaussian. We start by calculating the mean and variance of the distribution.

Proposition 2: For signals combining from N radios having independent zero mean Gaussian phase with variance σ_e^2 , the mean and the variance of the BF gains G are given by

$$\mathbb{E}\{G\} = 1 + (N-1)e^{-\sigma_e^2} \quad (27)$$

$$\text{var}\{G\} = \frac{(N-1)}{N}(1-e^{-\sigma_e^2})^2 \left((1-e^{-\sigma_e^2})^2 + 2Ne^{-\sigma_e^2} \right) \quad (28)$$

The proof is in Appendix B. Note that the mean was previously derived in [14]. In Fig. 2a, we plot the average BF gain using (27) as a function of σ_e with the error bars representing the standard deviation ($\sqrt{\text{var}\{G\}}$). For $\sigma_e = 0$, we get a BF gain of N as we ideally expect. As σ_e increases, the mean BF gains decrease and their variances increase and this happens faster for larger N . Thus when designing a BF system unless N and σ_e are small, we can not assume a perfect N fold power increase due to BF. To verify the derived mean and variance, for each value of N and σ_e , we sampled 100,000 zero mean Gaussian RVs of variance σ_e^2 for each radio and added them to calculate G numerically. The simulations shown in Fig.2a as

thick dashed lines with dashed error bars overlap the derived expressions verifying Proposition 2.

To better understand the variance behavior with N , for small σ_e^2 , we simplify (28) to get $\text{var}\{G\} \approx 2Ne^{-\sigma_e^2}(1 - e^{-\sigma_e^2})^2$. Thus the variance increases linearly with the number of slaves for small σ_e^2 . The linear relation between $\text{var}\{G\}$ and N is illustrated in Fig.2b. The higher the value of σ_e^2 , the larger the slope. The large discrepancy in the values of the variance with N shows the importance of considering the distribution of G and not just its mean in the design of reliable BF systems. Next, we approximate the distribution of G . First, we consider the case of large N using the central limit theorem. Then, we consider the case for a small N and small σ_e^2 and use the Taylor series to derive the approximation.

Proposition 3: For large N , the distribution of G tends to a Gaussian distribution with mean and variance given by Proposition 2.

Proposition 4: For small combined phase error variance σ_e^2 or for large N , the distribution of G can be approximated by $N - X_\gamma$ where X_γ is a random variable following the Gamma distribution $X_\gamma \sim \Gamma(K, \theta)$ with

$$K = \frac{N(N-1)}{(1 - e^{-\sigma_e^2})^2 + 2Ne^{-\sigma_e^2}} \quad (29)$$

$$\theta = \frac{1}{N}(1 - e^{-\sigma_e^2}) \left((1 - e^{-\sigma_e^2})^2 + 2Ne^{-\sigma_e^2} \right) \quad (30)$$

The proofs are in Appendices C and D respectively. We start by plotting the empirical cumulative distribution function (CDF) of G for small N and a small $\sigma_e = 0.1$ in Fig. 3a. We can see that the distribution is not Gaussian and is accurately approximated by the Gamma distribution. Then, we consider a large $N \geq 30$ and relatively large value of $\sigma_e = 1$ in Fig. 3b. From that Figure, we can see that all three CDFs overlap for large N and large σ_e verifying Prop. 3 and 4. Based on these results, since the Gamma distribution applies to a wider range of N and σ_e^2 , we use it later to approximate the BF gain distribution. Note that neither approximation is accurate for small values of N and a large value of σ_e^2 , however, in this regime the BF gains are small with a large variance, which is not of practical importance. It is important to note that the derived variance and distribution approximation in this section apply to any BF protocol where the phase error ϕ_n^e is independent for all n and can be approximated by zero-mean Gaussian RVs. For our protocol, the value of σ_e^2 can depend on N for scenarios where the BF overhead N_{ov} is constrained by the channel coherence time. In such scenarios, the duration of each preamble decreases as N increases to satisfy the fixed N_{ov} . Thus the estimators error variances and consequently σ_e^2 increase with N . The dependence between N and σ_e^2 is considered when designing the BF preambles in short coherence channels later in Section VIII-A.

VI. NUMERICAL AND EXPERIMENTAL VALIDATION

In this Section, after deriving the BF framework, we verify it numerically and experimentally and we show that it can be used to predict the BF gains at different SNRs. Using UAV experiments and emulation over a UAV channel trace,

TABLE II: Beamforming Waveform Specifications

Scenario	Parameters
Simulation	$N_{\text{ZC}} = 10, M = 63, t_{\text{syn}} = 0.63\text{ms}, t_{\text{ph}} = 0.1\text{ms}, t_{\text{fb}} = 0.1\text{ms}, t_{\text{g1}} = t_{\text{g2}} = t_{\text{g3}} = 1\text{ms}, t_{\text{p}} = 12\text{ms}, t_{\text{e}} = 9\text{ms}, t_{\text{cyc}} = 50\text{ms}$
Lab	$N_{\text{ZC}} = 10, M = 63, t_{\text{syn}} = 0.63\text{ms}, t_{\text{ph}} = 0.1\text{ms}, t_{\text{fb}} = 0.1\text{ms}, t_{\text{g1}} = 6\text{ms}, t_{\text{g2}} = 4\text{ms}, t_{\text{g3}} = 16\text{ms}, t_{\text{p}} = 10\text{ms}, t_{\text{cyc}} = 180\text{ms}$
UAV	$N_{\text{ZC}} = 10, M = 63, t_{\text{syn}} = 0.63\text{ms}, t_{\text{ph}} = 0.1\text{ms}, t_{\text{fb}} = 0.1\text{ms}, t_{\text{g1}} = 6\text{ms}, t_{\text{g2}} = 4\text{ms}, t_{\text{g3}} = 11\text{ms}, t_{\text{p}} = 1\text{ms}, t_{\text{cyc}} = 75\text{ms}$

we evaluate the impact of the channel coherence time on the BF gains.

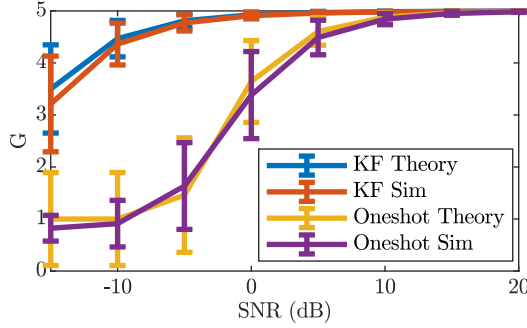
A. Numerical Validation

We simulated the BF protocol between a destination radio and N BF radios. During a BF cycle, signals transmitted from BF radio n to the destination is multiplied by $e^{j(2\pi f_n t + \phi_n)}$ with noise added to realize the SNR γ_{preBF} . Any signal transmitted the other way uses the negative value of f_n with noise added to realize the SNR γ_{DR} . At the start of each BF cycle, for BF slave n , we sample uniform random phase ϕ_n and f_n is generated using a discrete Wiener process as described in (15) having variance q . Since we are assuming that the signal is transmitted within the channel coherence time, both frequency and phase are assumed to be constant during the same BF cycle.

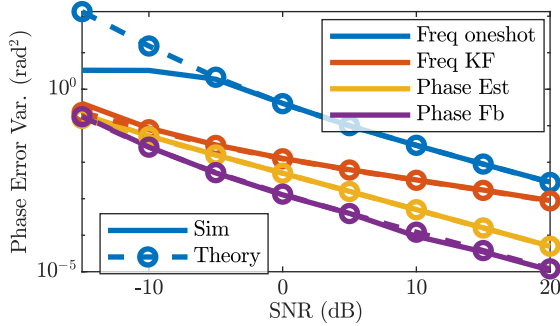
The signals transmitted follow the BF protocol. For phase estimation and feedback, we used the estimators discussed in Section IV and for frequency offset we either used the oneshot estimator from Section III-A alone or combined with KF. To avoid errors in measuring the BF gain, the combined signal magnitude was evaluated at time t_e before adding the noise.

In our simulations, we considered $N = 5$ BF radios using a sampling rate of 1MHz ($T_s = 1\mu\text{s}$). The exact duration of each preamble is given in the first row of Table II and we used $q = 0.18$. The evaluation time $t_e = 9\text{ms}$ is in the middle of the payload. One million BF cycles were simulated.

We start by discussing the results obtained when using the oneshot frequency estimation. The average BF gain obtained from simulations is plotted in Fig. 4a with the error bars representing its standard deviation. For the oneshot results, the theoretical value is obtained by calculating the variance of each estimator using (14), (24), and (26), calculating σ_e^2 using (12), then the BF gain mean and variance using Proposition 2. From that Figure, we can see that the theoretical mean matches the simulations to a large extent. As for the variances, they match except for SNRs below 0dB. By plotting a breakdown of the phase error for the slave $n = 3$ using (12) in Fig. 4b, we see that at SNRs below 0dB the theoretical oneshot frequency variance is overestimated. This happened because the phase error becomes uniform and the Gaussian assumption no longer holds leading to the discrepancy in Fig. 4a. At these low SNRs, the BF gains are negligible and this is not a useful BF design. From Fig. 4b, since the phase error from the frequency estimation error is dominant, it would be beneficial to allocate



(a) BF Gains using oneshot and KF for frequency synch. The standard dev. is shown as error bars.



(b) Phase error variance breakdown with respect to protocol stages.

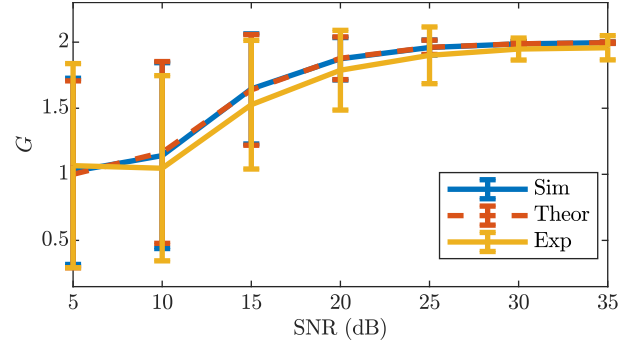
Fig. 4: Simulated BF Gains and phase errors at different SNRs for $N = 5$ using the waveform from Table II.

more time to frequency estimation or use the KF to reduce its variance.

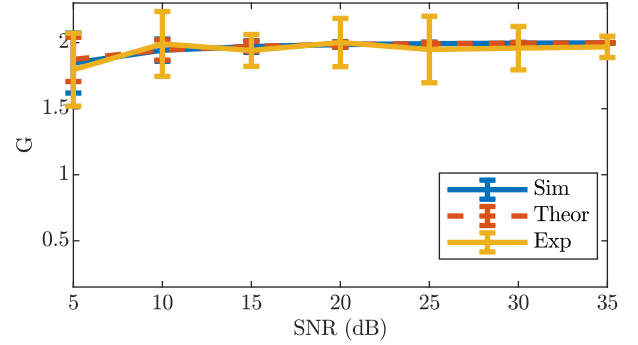
Next, we discuss the BF results when using KF using the same Figures 4a and 4b. The theoretical KF variance is calculated using (23) with the measurement variance r being the oneshot variance and q perfectly known. From Fig. 4a, we can see that both theoretical and simulated curves overlap. A small discrepancy exists at low SNR, which we attribute to an insufficient number of BF cycles. Since KF is a recursive filter, its output depends on all previous cycles and convergence is slower for high measurement noise variance [20]. Compared to the oneshot BF, at low SNR, KF provides significant BF gain improvements by reducing the frequency estimation variance and the resulting phase errors as shown in Fig. 4b. From that Figure, we also see that as the SNR (above 0dB) becomes larger, the gap between oneshot and KF decreases. This happens because as r decreases at high SNR, the ratio r/q becomes small and the benefit from using KF decreases.

B. Experimental Validation

The proposed BF protocol was implemented using three USRP B205-mini software-defined radios (SDR); two were used as BF radios and one as the destination radio. The destination radio initiates a BF cycle by transmitting the frequency synchronization preamble. The BF radios are always running the autocorrelation given by (13) and using its output power level to detect the preamble. Once detected, the frequency offset is estimated (using oneshot or KF) and corrected. Each BF



(a) BF gains using oneshot frequency estimation.



(b) BF gains using KF for frequency estimation.

Fig. 5: Experimental results collected using $N = 2$ BF software-defined-radios in a lab along with the theoretical results predicted by the BF framework and simulations.

radio transmits the phase estimation preamble in a preassigned time slot. The destination radio estimates the phase and feeds it back to the BF radios using the same previously discussed waveforms and estimators. Once the feedback is obtained, the radios transmit a known payload, which is received and stored by the destination. The payload consists of three parts; each of the two BF radio transmits individually at first, then both BF radios transmit simultaneously. The magnitude of each part of the payload is estimated by averaging, then the BF gain is calculated by dividing the power of the simultaneous transmission by the sum of the individual transmissions as per (5). All the signal processing was implemented using GNURadio [21] and timed burst transmissions were used for the different stages of the protocol. The destination processing was performed on a laptop and the BF radios on ODROID XU4 single board computers (SBC). We conducted the experiments in the lab and on UAVs at a frequency of 915MHz with a sampling period of $T_s = 1\mu s$.

1) *Lab Experiment:* We started by verifying our simulations in a lab environment with a favorable channel. The beamforming slaves were placed in proximity from each other, 2.5 meters away from the destination in an undisturbed line-of-sight environment with a measured coherence time of 0.3s and $q = 0.18$. Both the destination and BF radios were set to use the same transmit gain, which was varied in increments of 5dB to obtain different SNRs. At each SNR, 900 beamforming cycles were performed. The timing of the protocol is shown in Table II. Notice that the guard times are much longer than

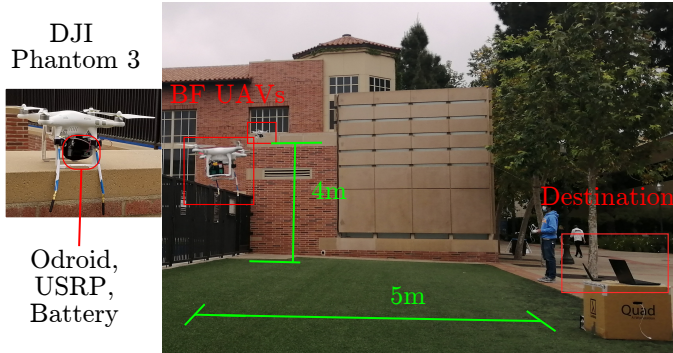


Fig. 6: The UAV experiment consists of 2 BF UAVs with SDRs mounted on-board. The UAVs were hovering freely and were not attached to the ground by wires.

TABLE III: BF UAV Results

Setup	Freq	SNR (dB)	G Mean	G Stdev
Ground	KF	26.9	1.825	0.319
Flying	oneshot	23.7	1.636	0.525
Flying	KF	24.9	1.632	0.438

in the simulations to allow the BF signal processing to operate in real-time, which makes t_e larger in (4), and thus increases σ_e^2 and degrades the BF gains.

The experimental results along with its simulated and theoretical equivalents are shown in Fig. 5a. We can see that the measured results are close to the simulation and theoretical results, which overlap. The improvement from using KF follows a similar trend to what was observed in Fig. 5b. This result experimentally verifies our simulation setup and analysis.

2) *UAV Experiment*: Next, we move our setup from the lab to UAVs. The BF radios, consisting of the SBC and USRPs along with a battery, were mounted on two DJI Phantom 3 drones as shown in Fig. 6. The destination radio was placed on the ground about 5m away from the UAVs which flew at a height of about 4m. The wind speed at the day of the experiment was 15Km/hr. Due to the wind and the noise of the UAV sensors, the UAVs were not stable and drifted within about a meter. The UAV operators frequently intervened to stabilize them.

Based on channel estimation performed before the experiment, the coherence time was estimated to be about $\tau_c = 85ms$. Thus, the lab experiment BF cycle ($t_{cyc} = 180ms$) is too long for the UAV channel. For the BF to work from the UAVs, the BF cycle was redesigned to have shorter guard times and a 10 times shorter payload as detailed in Table II, yielding a reduced $t_{cyc} = 75ms$, which is shorter than τ_c but only with a small margin. The experiment was performed with three settings: 1) UAVs were on the ground and used KF for frequency synchronization, 2) UAVs were flying and used oneshot for frequency synchronization and 3) UAVs were flying and used KF. The BF results are shown in Table III along with the average SNR. The BF UAVs attained about 80% of the ideal BF gains despite the low coherence time

channel. These gains are lower than the ground scenario as expected because of the shorter coherence time. As for the comparison between KF and oneshot, there is no significant difference because r/q is small; r is small because of the high SNR and q is large because of the short coherence time.

C. Emulation

To overcome the large delays of the BF implementation and have a fair comparison between KF and Oneshot, we emulated BF over a channel trace. The channel trace was obtained by capturing a repeating ZC sequence from a flying UAV over a period of 100s. Using this trace, we emulated the BF protocol as follows; we used a duration t_{syn} to estimate the frequency offset and corrected for it, then we estimated the phase offset after a delay equivalent to the protocol ($t_{g1} + Nt_{ph} + t_{g2}$) and corrected for it. The feedback stage was not emulated and was assumed to be ideal. At the evaluation time t_e , we estimated the phase error ϕ^e which for a static channel and perfect estimation should equal zero. The variance of ϕ^e calculated by emulation over the entire trace provides an estimate of σ_e^2 if BF was applied in this channel. Note that the channel trace was collected over one capture with a USRP operating in half-duplex. Hence, the emulation over that trace does not capture distortions due to burst transmissions and having both transmit and receive chains powered on simultaneously in the protocol implementation.

The measured phase errors are reported in Table IV. The first row emulates the timing used in the UAV experiment and using the value of $\tau_c = 85ms$, which is the true one, to calculate the KF q . The calculated phase error variance σ_e^2 is shown for KF and oneshot, and the theoretically predicted mean BF gain G using (27) and $N = 2$. Due to the more favorable half-duplex capture and the ideal feedback, the predicted emulation BF gains (≈ 1.7) are better than the measured ones (≈ 1.6). For the relatively long BF packets at a the high SNR of the capture, the predicted BF gains using both oneshot and KF are very close (1.725 and 1.723) similar to our experimental results. Yet the BF gains are still below 2 due to the long BF cycle, so in row 2, we emulate the protocol using a shorter cycle of 18ms by scaling down t_e and the phase delay. Using this shorter cycle, the BF gains increase significantly for both KF and oneshot and approach the ideal gain of 2. This is the result we would expect using an optimized implementation of the BF protocol having shorter guard times. Due to the high SNR, both KF and oneshot still give a similar performance. Then in row 3, we added Gaussian noise to the channel trace to make its SNR drop to 0dB. The expected BF gains for KF become significantly better than those from oneshot. This result shows that if $t_{cyc} \ll \tau_c$, KF can attain significantly higher BF gains than oneshot for distantly deployed UAVs.

VII. BEAMFORMING SYSTEM DESIGN

After verifying the framework, we discuss how it can be used in designing BF systems. To design a reliable BF system, we need to specify the number of BF radios N and the duration of the preambles to exceed a minimum post-BF SNR with a given probability. The design procedure is over two steps; first

TABLE IV: BF Emulation over UAV Channel Trace

#	SNR	t_{cyc}	τ_c	KF σ_e^2 [G]	Onesh. σ_e^2 [G]
1	24dB	75ms	85ms	0.569 [1.725]	0.567 [1.723]
2	24dB	18ms	85ms	0.11 [1.99]	0.141 [1.98]
3	0dB	18ms	85ms	0.573 [1.85]	0.4 [1.72]

we determine N and σ_e^2 that meet the requirements and then we design the preambles' lengths to realize σ_e^2 at a given pre-BF SNR. Later in Section VIII, we apply the proposed design procedures for specific scenarios.

A. Specifying N and σ_e^2

Although the pre-BF SNR (γ_{preBF}) is assumed constant, due to the phase error variance, the post BF SNR (γ_{postBF}) varies randomly. A reliable BF system has to exceed a specified outage probability p_{out} such that $P(\gamma_{\text{postBF}} < \gamma_{\text{min}}) \leq p_{\text{out}}$, where γ_{min} is the minimum SNR. Using the gamma approximation of the BF gain distribution and the post-BF SNR definition (8), we can rewrite $P(\gamma_{\text{postBF}} < \gamma_{\text{min}}) = 1 - F_{X_\gamma}\left(N - \frac{\gamma_{\text{min}}}{\gamma_{\text{preBF}}N}\right)$ where $F_{X_\gamma}(x)$ is the CDF of the Gamma distribution from Proposition 4 whose mean and variance depend on N and σ_e^2 . Hence, our objective is to determine N and σ_e^2 which satisfy

$$F_{X_\gamma}\left(N - \frac{\gamma_{\text{min}}}{\gamma_{\text{preBF}}N}\right) \leq 1 - p_{\text{out}} \quad (31)$$

We know the distribution of X_γ and how N and σ_e^2 affect it, however, inverting (31) to obtain an explicit relation between N and σ_e^2 is intractable. The fact that σ_e^2 can depend on N under fixed BF overheads further complicates analytical solutions. It is easy, however, to check whether a given choice of N and the corresponding σ_e^2 satisfies the requirements given by (31). Thus, we resort to numerical trial-and-error methods to find N and σ_e^2 satisfying the requirements. The exact method depends on the scenario and whether N is fixed or not, and thus its discussion is deferred to Section VIII where example scenarios are presented.

B. Beamforming Signals Design

For given values of N , γ_{preBF} , and γ_{DR} , we want to optimize the time allocated to each preamble for σ_e^2 to meet the system requirements. We identify two problems of interest; the first one is to minimize σ_e^2 for limited BF overheads and the second problem is to minimize the BF overheads N_{ov} to meet a maximum allowable phase error variance. The first problem is suitable for short coherence time channels, where the BF overheads are constrained to allow time for communication within the coherence time. The second problem, on the other hand, is suited for relatively large coherence time channels, where large BF overheads are possible. An example of each problem is provided later in Section VIII.

Next, we formulate both problems. The total overheads in samples defined in (11) can be written as a function of the duration of each stage $N_{\text{ov}}(N_{\text{syn}}, N_{\text{ph}}, N_{\text{fb}})$. For fixed N , γ_{preBF} and γ_{DR} , the phase variance σ_e^2 becomes a function of the

number of samples allocated to each stage $\sigma_e^2(N_{\text{syn}}, N_{\text{ph}}, N_{\text{fb}})$ defined as

$$\sigma_e^2(N_{\text{syn}}, N_{\text{ph}}, N_{\text{fb}}) = (2\pi t_e)^2 \sigma_f^2 + \sigma_{ph}^2 + \sigma_{fb}^2 \quad (32)$$

The values of σ_f^2 , σ_{ph}^2 , and σ_{fb}^2 are dependent on the choice of estimators and are a function of N_{syn} , N_{ph} , and N_{fb} respectively. For our choice of estimators $\sigma_{ph}^2 = \sigma_{phe}^2$ defined by (24), and $\sigma_{fb}^2 = \sigma_{fbe}^2$ defined by (26). As for the frequency error variance, if we use oneshot estimation $\sigma_f^2 = \sigma_{fe}^2$ as defined by (14) and if we use the KF $\sigma_f^2 = \sigma_{fk}^2$ as defined by (23) with $r = \sigma_{fe}^2$.

Note that for a chosen Zadoff-Chu sequence of a length M , we can only optimize the number of repetitions N_{ZC} to change N_{syn} . Hence, for fixed N , the problem P1 can be written as

$$\begin{aligned} \text{P1 : minimize} \quad & \sigma_e^2(N_{\text{ZC}}M, N_{\text{ph}}, N_{\text{fb}}) \quad (33) \\ \text{subject to} \quad & N_{\text{ov}}(N_{\text{ZC}}M, N_{\text{ph}}, N_{\text{fb}}) \leq \delta_{N_{\text{ov}}} \\ & N_{\text{ZC}}, N_{\text{ph}}, N_{\text{fb}} \in \mathbb{Z}^+, \quad N_{\text{ZC}} \geq 2 \quad (34) \end{aligned}$$

where $\delta_{N_{\text{ov}}}$ is maximum overhead length which depends on the channel coherence time, and \mathbb{Z}^+ is the set of positive integers. For a maximum allowable phase error $\delta_{\sigma_e^2}$, the second problem P2 can be written as

$$\begin{aligned} \text{P2 : minimize} \quad & N_{\text{ov}}(N_{\text{ZC}}M, N_{\text{ph}}, N_{\text{fb}}) \quad (35) \\ \text{subject to} \quad & \sigma_e^2(N_{\text{ZC}}M, N_{\text{ph}}, N_{\text{fb}}) \leq \delta_{\sigma_e^2} \\ & N_{\text{ZC}}, N_{\text{ph}}, N_{\text{fb}} \in \mathbb{Z}^+, \quad N_{\text{ZC}} \geq 2 \quad (36) \end{aligned}$$

Then, we argue that for our choice of estimators, both problems are convex with respect to their variables and thus are easy to solve. Except for the KF, all these estimators take the form $f(x) = \frac{c_1}{x} + \frac{c_2}{x^2}$ with respect to their variables for some positive c_1 and c_2 where x is strictly positive, hence they are all convex over their domain. As for the KF, when substituting for r , it takes the form $f(x) = c_1 + \sqrt{c_2 + \frac{c_3}{x} + \frac{c_4}{x^2}}$ with respect to its positive variable x for some positive c_1 , c_2 , c_3 and c_4 . This can be rewritten as $f(x) = c_1 + \|\mathbf{y}\|$ where $\mathbf{y} = [\sqrt{c_2}, \frac{\sqrt{c_3}}{\sqrt{x}}, \frac{\sqrt{c_4}}{x}]^T$. The norm is convex and non decreasing and $\frac{\sqrt{c_3}}{\sqrt{x}}$ and $\frac{\sqrt{c_4}}{x}$ are convex for positive x . By applying the composition rule [22], the KF variance is convex. Hence, $\sigma_e^2(N_{\text{ZC}}M, N_{\text{ph}}, N_{\text{fb}})$ is convex with respect to its arguments for all of our estimators. As for $N_{\text{ov}}(N_{\text{ZC}}M, N_{\text{ph}}, N_{\text{fb}})$, it is an affine combination of its arguments. This makes both problems P1 and P2 integer convex problems, which can be optimally solved using CVX with a mixed integer solver [23].

VIII. BEAMFORMING DESIGN SCENARIOS

The proposed BF framework and the derived relations can be applied to many BF scenarios. In this section, we discuss the design procedures for two example scenarios. In the first example, we consider a large swarm of small UAVs; we want to determine the minimum N to satisfy the SNR requirements. Due to the UAVs' high mobility, the channel coherence time is small and the BF overheads are constrained. This example maps to the problem P1. In the second example, we consider

$N = 4$ weather balloons sending short payloads. Due to the long coherence time resulting from the balloons slow motion, large BF overheads are possible. However, to avoid energy wasted on unneeded transmission, our objective is to minimize the BF overheads while satisfying the SNR requirement. This example maps to the problem P2.

A. Swarm of Small UAVs

A swarm of N_{ub} small UAVs is deployed in an urban environment for an application like crowd monitoring [24]. A large number of small UAVs is deployed and they continuously transmit data. To avoid a large overhead in data sharing among UAVs for BF, we want to determine the minimum number of UAVs to beamform such that the destination SNR exceeds a minimum of $\gamma_{\text{min}} = 5\text{dB}$ for 90% of the time ($p_{\text{out}} = 0.1$).

For the urban channel, we consider a channel having a path loss coefficient of 3.7 [25] and a coherence time of 10ms [26]. The maximum transmit power of each UAV is $P_T = 0\text{dBm}$ and of the destination $P_T^D = 20\text{dBm}$. Communication takes place over a frequency of 915MHz using a sampling time of $T_s = 1\mu\text{s}$ and a BW of 1MHz and all radios have a noise figure of 3dB. By performing the link budget calculation, the SNR from an individual UAV at 1Km is close to -13dB, so the minimum required BF gain is $G_{\text{req}} = 18\text{dB}$. Assuming ideal BF gain of N^2 , the required gain can be achieved using only 8 BF radios. However, due to the short coherence time, the entire BF packet is assumed to be limited to 5ms and based on the payload required by the application only 1ms of BF overhead is allowed. At this low SNR and with this short BF overhead, the ideal beamforming gains are not achievable and large BF variance is expected. We need to use more than 8 BF radios so that the SNR exceeds 5dB for 90% of the time as required. Our objective is to determine the minimum N and the duration of each preamble.

We use our analytical framework to find the minimum N . Since for fixed overheads N_{ov} , σ_e^2 depends on N , we need to solve P1 to calculate σ_e^2 for each N . The proposed approach is summarized in Algorithm 1 and it works as follows; we start from the lower bound on N , which occurs when assuming ideal BF $N_{\text{lb}} = \lceil \sqrt{G_{\text{req}}} \rceil$ and increment N until the requirement is satisfied. For each N , we solve the minimum phase error problem P1 to obtain σ_e^2 . Using the resulting σ_e^2 , we substitute in (31) to determine if the requirement is satisfied or not. The first N satisfying the requirement is the minimum N meeting the SNR requirements. If the maximum number of available BF radios N_{ub} was reached without satisfying (31), another approach needs to be considered to meet the requirements like increasing the BF overhead or the transmit power of the radios. Since the BF is performed periodically and $t_{\text{cyc}} < \tau_c$, we assume that KF is used for frequency tracking.

The calculated N for different distances is shown in Fig. 7a along with N_{lb} calculated assuming ideal BF gain. To verify that the obtained solution meets our design criteria, we simulated 10K BF cycles of the BF protocol using the calculated N and the optimized waveforms obtained from P1 at each distance. The destination SNR was measured and its empirical CDF for the proposed N and the ideal N_{lb} are plotted

Algorithm 1:

input : $N_{\text{lb}}, N_{\text{ub}}, N_{\text{ov}}, p_{\text{out}}, \gamma_{\text{min}}$
output: Solved, N , BF waveform
Solved := False ;
for $n_i = N_{\text{lb}}$ to N_{ub} **do**
 Solve P1 to determine σ_e^2 ;
 if n_i and σ_e^2 satisfy (31) **then**
 Set Solved to True, N to n_i , and BF waveform
 to solution of P1, and exit ;
 end
end

in Fig. 7b and 7c respectively. From these Figures, we see that the required outage probability is met using the proposed N . Thus, our problem solution and the underlying analysis can be used to design reliable BF systems satisfying the design requirements as verified by simulations. On the other hand, relying on the ideal N_{lb} is expected to yield lower BF gains than the desired ones in realistic deployment scenarios.

B. Weather Balloons

Weather balloons are deployed at high altitudes to perform atmospheric measurements and report them back to the ground. We consider $N = 4$ weather balloons deployed at a distance of 50KM from the destination radio. Due to their high altitude, the channel is dominated by line-of-sight propagation and we consider a path loss coefficient of 2 and a large channel coherence time exceeding 100ms. The large channel coherence time allows for much longer BF overheads. However, to economize the balloon payload battery power, we want to minimize the transmission time. Our objective is to determine the smallest BF overheads to attain a received SNR exceeding a minimum of $\gamma_{\text{min}} = 5\text{dB}$ for 90% of the time ($p_{\text{out}} = 0.1$). We use the same power, frequency, bandwidth, and noise parameters as the previous scenario except $P_T = 10\text{dBm}$ is larger. The SNR from a single radio is -4.6dB and thus the required BF gain at 50KM distance is 9.6dB. Assuming that the measurements are infrequent and not periodic, we use oneshot frequency estimation.

To design this system, we find the minimum phase error needed to satisfy the requirement ($\delta_{\sigma_e^2}$), then we find the shortest overhead to meet this phase error. Since, for fixed N , increasing σ_e^2 decreases the average BF gain and vice versa, we determine $\delta_{\sigma_e^2}$ by applying the bisection method on (31). Then, using $\delta_{\sigma_e^2}$, we solve the problem P2 to determine the minimum overhead. If the minimum overhead makes the BF packet exceed the channel coherence time, the solution is not valid and we need to consider another alternative like increasing the transmit power. The minimum overheads obtained are shown in Fig. 8a for different distances. Then, we simulated the BF protocol at these SNRs using the waveforms obtained from P2 and plotted the empirical CDF of the destination SNR in Fig. 8b. We can see that the proposed solution approach meets the required outage probability, which verifies the solution and all the underlying analysis.

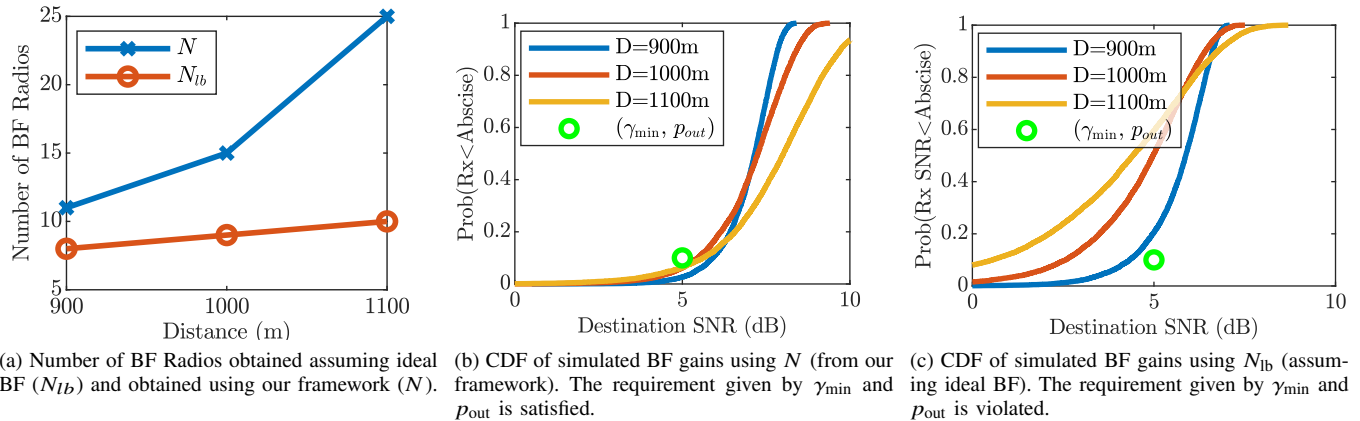


Fig. 7: Results for minimizing N in a swarm of small UAVs assuming a fixed BF overhead. Using N obtained from our approach, the SNR requirement is satisfied as verified by simulations.

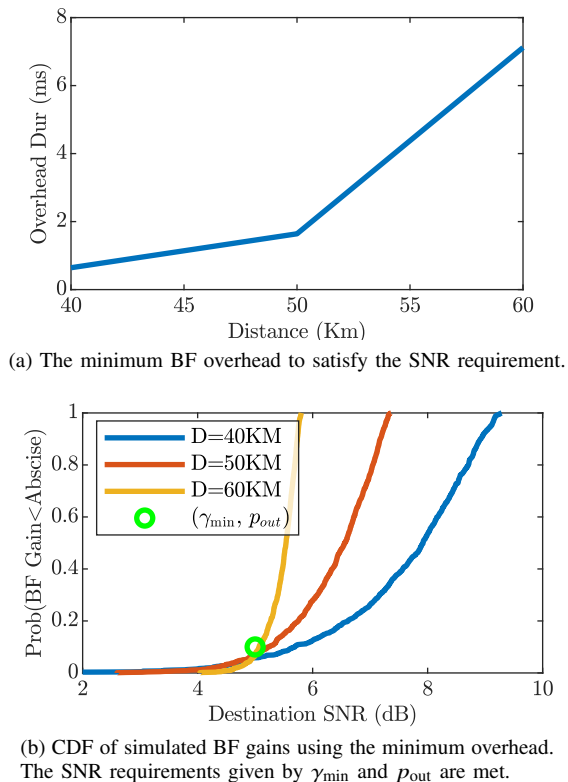


Fig. 8: For $N = 4$ weather balloons, in a long coherence time channel, the minimum overheads obtained using our framework satisfy the SNR requirements.

IX. CONCLUSION

In this work, we developed and verified a mathematical framework to model the BF performance for a destination-led BF protocol. The BF gains distribution was approximated by a gamma distribution assuming a zero mean normally distributed combining phase errors and the proposed distribution was verified using simulations. The effect of the pre-BF SNR and the preamble lengths on the combining phase error was derived for our choice of estimators. Using software-defined radios, in

a lab, we experimentally verified the predictions of our BF framework. The BF radios were mounted on UAVs and were shown to exceed 80% of the ideal BF gains despite the low coherence time channel. The proposed framework can be used to design BF systems for a given deployment as illustrated by two example scenarios.

Even though we only considered a specific BF protocol and only two example scenarios, the proposed framework can support many protocol variations and use cases. For the protocol, the framework is applicable for any other choice of estimators as long as their phase variance can be expressed mathematically. As for the scenarios, heuristics can easily be developed to optimize over a combination of the SNR, preamble lengths, and the number of BF slaves, enabling the framework to adapt to many different deployment scenarios.

APPENDIX

A. Proof of Proposition 1

The variance error of the KF output is given by $p_{k|k}$ and we want to calculate its value. Substituting (17) into (21), we get $p_{k+1|k} = \frac{r p_{k|k-1}}{p_{k|k-1} + r} + q$. At steady state $p_{k+1|k} = p$ for all k and we get a simple form of the algebraic Riccati equation $p = \frac{r p}{p+r} + q$ [27]. Solving the equation, we get $p_{k+1|k} = p = \frac{q+r\sqrt{1+4\frac{r}{q}}}{2}$. Using (21), we get $\sigma_{fk}^2 = p_{k|k} = \frac{-q+q\sqrt{1+4\frac{r}{q}}}{2}$.

B. Proof of Proposition 2

$$\begin{aligned} G &= \frac{1}{N} \left| \sum_{n=1}^N e^{j\phi_n^e} \right|^2 = \frac{1}{N} \sum_{n=1}^N e^{j\phi_n^e} \sum_{m=1}^N e^{-j\phi_m^e} \\ &= 1 + \frac{2}{N} \sum_{m=1}^N \sum_{n=m+1}^N \cos(\phi_n^e - \phi_m^e) \end{aligned} \quad (37)$$

Using the fact that for a zero mean Gaussian RV x , $\mathbb{E}\{\cos x\} = e^{-\text{var}\{x\}/2}$ [14], we get

$$\mathbb{E}\{G\} = 1 + (N-1)e^{-\sigma_e^2} \quad (38)$$

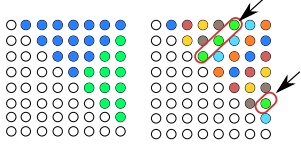


Fig. 9: Summation order for the matrix \mathbf{X} .

$$\begin{aligned}
 \text{var}\{G\} &= \frac{4}{N^2} \text{var}\left\{\sum_{m=1}^N \sum_{i=m+1}^N \cos(\phi_i^e - \phi_m^e)\right\} \\
 &= \frac{4}{N^2} \sum_{m=1}^N \sum_{i=m+1}^N \text{var}\{\cos(\phi_i^e - \phi_m^e)\} \\
 &\quad + \frac{8}{N^2} \sum_{m=1}^N \sum_{i=m+1}^N \sum_{p=i+1}^N \text{cov}\{\cos(\phi_i^e - \phi_m^e), \cos(\phi_m^e - \phi_p^e)\} \\
 &= \frac{(N-1)}{N} (e^{-\sigma_e^2} - 1)^2 \left((e^{-\sigma_e^2} - 1)^2 + 2Ne^{-\sigma_e^2} \right)
 \end{aligned} \tag{39}$$

where $\text{cov}\{x, y\}$ denotes the covariance of RVs x, y . Line (40) was obtained using the fact that $\text{var}\{\sum_{m=1}^M x_m\} = \sum_{m=1}^M \text{var}\{x_m\} + 2 \sum_{m=1}^M \sum_{n=m+1}^M \text{cov}\{x_m, x_n\}$ for any correlated M RVs x_m and by simplifying the summations. Line (41) uses the fact that for a zero mean Gaussian RV $\text{var}\{\cos x\} = \frac{1}{2}(e^{-\text{var}\{x\}} - 1)^2$ [14] and using that $\text{cov}\{\cos(\phi_i^e - \phi_m^e), \cos(\phi_m^e - \phi_p^e)\} = 0.5e^{-3\sigma_e^2} + 0.5e^{-\sigma_e^2} - e^{-2\sigma_e^2}$ as can be shown using the Gaussian RV relations from [14], the definition of covariance, and some trigonometric identities.

C. Proof of Proposition 3

We start by considering the simplified definition of G from (37). We rewrite the elements of the summation as the $N \times N$ matrix \mathbf{X} , such that its element $\mathbf{X}_{m,n} = \frac{2}{N} \cos(\phi_m - \phi_n)$. This yields $G = 1 + \sum_{m=1}^N \sum_{n=m+1}^N \mathbf{X}_{m,n}$. The summation is over the upper diagonal elements of the matrix. Our objective is to rewrite the inner sum as independent RVs of length proportional to N to invoke the central limit theory (CLT). To achieve that, we must avoid reusing the same value of ϕ_n^e in the inner sum, that is, the inner sum elements should have unique column and row indices.

$$\sum_{m=1}^N \sum_{n=m+1}^N \mathbf{X}_{m,n} = \sum_{n=2}^N \sum_{m=1}^{n-1} \mathbf{X}_{m,n} \tag{42}$$

$$= \sum_{n=2}^N \sum_{m=1}^{\min(n-1, N-n+1)} \mathbf{X}_{m,n} + \sum_{n=N/2+1}^N \sum_{m=N-n+1}^{n-1} \mathbf{X}_{m,n} \tag{43}$$

$$= \sum_{n=2}^N \left(\sum_{m=1}^{\lfloor n/2 \rfloor} \mathbf{X}_{m,n-m+1} + \sum_{m=1}^{\lfloor (N+1-n)/2 \rfloor} \mathbf{X}_{N+1-(n-m+1), (N+1)-m} \right) \tag{44}$$

The summation in (42) rewrites the equation from column wise to row wise. In Line (43), we split the elements of the summation at the upward diagonal as illustrated in the first image of Fig. 9 for an 8×8 matrix. In Line (44), the inner summation is rewritten as two summations over the upward diagonal elements as shown in different colors in the

second image of Fig. 9. From (44), each element of the inner summation consists of about $N/2$ terms¹ and none of the terms have common rows or columns, thus consist of independent RVs. We can rewrite the inner sum as the RV b_n as follows

$$b_n = \sum_{m=1}^{\lfloor n/2 \rfloor} \mathbf{X}_{m,n-m+1} + \sum_{m=1}^{\lfloor (N+1-n)/2 \rfloor} \mathbf{X}_{N+1-(n-m+1), (N+1)-m} \tag{45}$$

The variable b_n consists of identical independent RVs. Hence, for large N , the distribution of b_n converges to a Gaussian distribution. Lastly, we can rewrite G as

$$G = 1 + \sum_{n=2}^N b_n \tag{46}$$

The variables b_n are correlated Gaussian RVs, hence their sum is Gaussian. This proves that for large N , G is Gaussian and its mean and variance are given by Proposition 2.

D. Proof of Proposition 4

We start this proof by considering the case of small σ_e^2 and then discuss the case of large N . Since ϕ_n are zero mean and assuming small σ_e^2 , $\phi_m - \phi_n$ is typically small and we can use the Taylor expansion of cosine around zero to simplify $\mathbf{X}_{m,n}$ (as defined in Appendix C) as $\mathbf{X}_{m,n} \approx \frac{2}{N} \left(1 - \frac{(\phi_m - \phi_n)^2}{2} \right)$. Then, we can rewrite (45) as $b_n = 2 \frac{s_n}{N} - \chi_n$ where $s_n = \lfloor n/2 \rfloor + \lfloor (N+1-n)/2 \rfloor$ is the number of elements of b_n and $\chi_n = \frac{1}{N} \sum_{r=1}^{s_n} (\phi_{m_r} - \phi_{n_r})^2$ with m_r and n_r corresponding to the indexes from (45). The summation in χ_n is over independent zero mean Gaussian RVs that are squared, hence χ_n follows the Chi-squared distribution. We can rewrite G as

$$G = 1 + \frac{2}{N} \frac{N(N-1)}{2} - \sum_{n=2}^N \chi_n = N - X_\gamma \tag{47}$$

where $X_\gamma = \sum_{n=2}^N \chi_n$ is the sum of correlated Chi-squared RVs. The distribution of the summation of correlated Chi-squared RVs can be obtained using the Gamma distribution [28]. The shape K and scale θ parametrization of the resulting Gamma distribution can be calculated to realize the mean and variance of X_γ [29]. Using the mean and variance of G from Proposition 2, we get the following equations for the mean and variance respectively

$$K\theta = N - 1 - (N-1)e^{-\sigma_e^2} \tag{48}$$

$$K\theta^2 = \frac{(N-1)}{N} (1 - e^{-\sigma_e^2})^2 \left((1 - e^{-\sigma_e^2})^2 + 2Ne^{-\sigma_e^2} \right) \tag{49}$$

Solving these two equations, we get the values of K and θ in (29) and (30). This proof is based on the assumption that σ_e^2 is small. For large values of N , K becomes large, and the Gamma distribution converges to a Gaussian distribution with mean $K\theta$ and variance $K\theta^2$ [30], which is the true distribution of G as shown in Proposition 3.

¹For odd N , the number of elements is either $N/2$ or $N/2 - 1$. This difference is insignificant for large N .

REFERENCES

- [1] R. Mudumbai, G. Barriac, and U. Madhow, "On the Feasibility of Distributed Beamforming in Wireless Networks," *Trans. Wireless. Comm.*, vol. 6, no. 5, pp. 1754–1763, May 2007.
- [2] R. Mudumbai, D. Brown, U. Madhow, and H. Poor, "Distributed transmit beamforming: Challenges and recent progress," *IEEE Communications Magazine*, vol. 47, no. 2, pp. 102–110, Feb. 2009.
- [3] S. Jayaprakasam, S. K. A. Rahim, and C. Y. Leow, "Distributed and Collaborative Beamforming in Wireless Sensor Networks: Classifications, Trends, and Research Directions," *IEEE Communications Surveys Tutorials*, vol. 19, no. 4, pp. 2092–2116, Fourthquarter 2017.
- [4] S. Mohanti, C. Bocanegra, J. Meyer, G. Secinti, M. Diddi, H. Singh, and K. Chowdhury, "AirBeam: Experimental Demonstration of Distributed Beamforming by a Swarm of UAVs," in *2019 IEEE 16th International Conference on Mobile Ad Hoc and Sensor Systems (MASS)*, Nov. 2019, pp. 162–170.
- [5] Yung-Szu Tu and G. J. Pottie, "Coherent cooperative transmission from multiple adjacent antennas to a distant stationary antenna through AWGN channels," in *Vehicular Technology Conference. IEEE 55th Vehicular Technology Conference. VTC Spring 2002 (Cat. No.02CH37367)*, vol. 1, May 2002, pp. 130–134 vol.1.
- [6] R. Mudumbai, J. Hespanha, U. Madhow, and G. Barriac, "Distributed Transmit Beamforming Using Feedback Control," *IEEE Transactions on Information Theory*, vol. 56, no. 1, pp. 411–426, Jan. 2010.
- [7] D. R. B. III and H. V. Poor, "Time-Slotted Round-Trip Carrier Synchronization for Distributed Beamforming," *IEEE Transactions on Signal Processing*, vol. 56, no. 11, pp. 5630–5643, Nov. 2008.
- [8] S. Hanna, E. Krijestorac, and D. Cabric, "Feedback Free Distributed Transmit Beamforming using Guided Directionality," *arXiv:2108.01837 [eess]*, Aug. 2021.
- [9] S. Leak, I. Grivell, H. Suzuki, C. K. Sung, M. Hedley, G. Lechner, M. Lavenant, H. Soetiyono, and D. Kramarev, "Distributed Transmit Beamforming Expanding the Capacity and Range of Tactical Communications," in *2018 Military Communications and Information Systems Conference (MilCIS)*, Nov. 2018, pp. 1–6.
- [10] D. Kramarev, I. Ahmad, K. Layton, M. Lavenant, H. Soetiyono, G. Lechner, H. Suzuki, I. Grivell, and S. Leak, "Event-Triggered Synchronization for Mobile Distributed Transmit Beamforming," in *MILCOM 2019 - 2019 IEEE Military Communications Conference (MILCOM)*, Nov. 2019, pp. 343–348.
- [11] M. M. Rahman, H. E. Baidoo-Williams, R. Mudumbai, and S. Dasgupta, "Fully Wireless Implementation of Distributed Beamforming on a Software-defined Radio Platform," in *Proceedings of the 11th International Conference on Information Processing in Sensor Networks*, ser. IPSN '12. New York, NY, USA: ACM, 2012, pp. 305–316.
- [12] F. Quitin, U. Madhow, M. M. U. Rahman, and R. Mudumbai, "Demonstrating distributed transmit beamforming with software-defined radios," in *2012 IEEE International Symposium on a World of Wireless, Mobile and Multimedia Networks (WoWMoM)*, Jun. 2012, pp. 1–3.
- [13] F. Quitin, M. M. U. Rahman, R. Mudumbai, and U. Madhow, "A Scalable Architecture for Distributed Transmit Beamforming with Commodity Radios: Design and Proof of Concept," *IEEE Transactions on Wireless Communications*, vol. 12, no. 3, pp. 1418–1428, Mar. 2013.
- [14] D. Richard Brown, P. Bidigare, and U. Madhow, "Receiver-coordinated distributed transmit beamforming with kinematic tracking," in *2012 IEEE International Conference on Acoustics, Speech and Signal Processing*, Mar. 2012, pp. 5209–5212.
- [15] B. Williams and T. Camp, "Comparison of Broadcasting Techniques for Mobile Ad Hoc Networks," in *Proceedings of the 3rd ACM International Symposium on Mobile Ad Hoc Networking & Computing*, ser. MobiHoc '02. New York, NY, USA: ACM, 2002, pp. 194–205.
- [16] H. Yan, S. Hanna, K. Balke, R. Gupta, and D. Cabric, "Software Defined Radio Implementation of Carrier and Timing Synchronization for Distributed Arrays," in *2019 IEEE Aerospace Conference*, Mar. 2019, pp. 1–12.
- [17] G. W. Lank, I. S. Reed, and G. E. Pollon, "A Semicoherent Detection and Doppler Estimation Statistic," *IEEE Transactions on Aerospace and Electronic Systems*, vol. AES-9, no. 2, pp. 151–165, Mar. 1973.
- [18] N. A. Thacker and A. Lacey, "Tutorial: The kalman filter," *Imaging Science and Biomedical Engineering Division, Medical School, University of Manchester*, p. 61, 1998.
- [19] S. Tretter, "Estimating the frequency of a noisy sinusoid by linear regression (Corresp.)," *IEEE Transactions on Information Theory*, vol. 31, no. 6, pp. 832–835, Nov. 1985.
- [20] L. Cao and H. M. Schwartz, "Exponential convergence of the Kalman filter based parameter estimation algorithm," *International Journal of Adaptive Control and Signal Processing*, vol. 17, no. 10, pp. 763–783, 2003.
- [21] GNU Radio Website, "GNU Radio," <https://gnuradio.org/>.
- [22] S. Boyd and L. Vandenberghe, *Convex Optimization*. Cambridge university press, 2004.
- [23] M. Grant and S. Boyd, *CVX: Matlab Software for Disciplined Convex Programming, Version 2.1*, Mar. 2014.
- [24] A. Trotta, U. Muncuk, M. Di Felice, and K. R. Chowdhury, "Persistent Crowd Tracking Using Unmanned Aerial Vehicle Swarms: A Novel Framework for Energy and Mobility Management," *IEEE Vehicular Technology Magazine*, vol. 15, no. 2, pp. 96–103, Jun. 2020.
- [25] A. Goldsmith, *Wireless Communications*. Cambridge university press, 2005.
- [26] Y. Chakkour, H. Fernández, V. M. R. Peñarrocha, L. Rubio, and J. Reig, "Coherence Time and Doppler Spread Analysis of the V2V Channel in Highway and Urban Environments," in *2018 IEEE International Symposium on Antennas and Propagation USNC/URSI National Radio Science Meeting*, Jul. 2018, pp. 373–374.
- [27] D. P. Bertsekas, *Dynamic Programming and Optimal Control: Vol. 1*. Athena scientific Belmont, 2000.
- [28] N. H. Gordon and P. F. Ramig, "Cumulative distribution function of the sum of correlated chi-squared random variables," *Journal of Statistical Computation and Simulation*, vol. 17, no. 1, pp. 1–9, Jan. 1983.
- [29] A. Ferrari, "A note on sum and difference of correlated chi-squared variables," *arXiv:1906.09982 [math, stat]*, Jun. 2019.
- [30] A. DasGupta, *Normal Approximations and the Central Limit Theorem*. New York, NY: Springer, 2010, pp. 213–242.